J Mater Sci (2011) 46:7039–7045
DOI 10.1007/s10853-011-5672-8

Experimental determination and thermodynamic modeling of phase equilibria in the Cu–Cr system

Z. M. Zhou · J. Gao · F. Li · Y. P. Wang · M. Kolbe

Received: 15 April 2011 / Accepted: 30 May 2011 / Published online: 8 June 2011

Abstract Liquidus temperatures in the Cu–Cr system at compositions of 10.0–72.7 at.% Cr were determined using electromagnetic levitation melting. The present data agree with the prediction of a recent thermodynamic study of the system for compositions up to 20.0 at.% Cr. However, they show large and positive deviations for other compositions. Microscopic studies reveal that compositions between 10.0 and 50.5 at.% Cr solidified into a dendritic microstructure, whereas those between 55.9 and 72.7 at.% Cr solidified into a droplet-shaped microstructure. The microstructure of the latter type provides direct evidence for the existence of a stable miscibility gap over Cr-rich compositions. Phase equilibria in the Cu–Cr system were calculated using the CALPHAD method. A novel phase diagram was proposed for the Cu–Cr system, which shows a monotectic reaction between compositions of 50.8 and 83.2 at.% Cr at an invariant temperature of 2020 ± 22 K. The novel phase diagram has reduced the discrepancies between the literature data.

Z. M. Zhou · J. Gao (✉) · F. Li
Key Laboratory of Electromagnetic Processing of Materials (Ministry of Education), Northeastern University, Shenyang 110004, China
e-mail: jgao@mail.neu.edu.cn

Z. M. Zhou · Y. P. Wang
Institute of Metal Research, Chinese Academy of Sciences, Shenyang 110016, China

Y. P. Wang
School of Science, Xi'an Jiaotong University, Xi'an 710049, China

M. Kolbe
Institut für Materialphysik im Weltraum, Deutsches Zentrum für Luft-und Raumfahrt (DLR), 51170 Köln, Germany

Present Address:
Z. M. Zhou
Department of Materials Science and Engineering, Chongqing University of Technology, 400050 Chongqing, China

Introduction

The Cu–Cr system does not form any intermetallic compounds under equilibrium or non-equilibrium conditions. The mutual solubility of two terminal solutions is low at room temperature. For these reasons, Cu–Cr compositions up to 55 at.% Cr exhibit a combination of high mechanical strength with high electrical conductivities, which is attractive in many industrial applications [1, 2]. An accurate knowledge of phase equilibria is of fundamental and technical interest. However, it has turned out difficult to investigate phase equilibria in the Cu–Cr system because of a high melting point and a strong oxidation tendency of elemental Cr.

Few experimental studies [3–6] suggested that the Cu–Cr system falls into a monotectic type with a stable miscibility gap. Owing to the use of impure raw materials or occurrence of melt contamination in these studies, phase diagrams of the monotectic type have been generally questioned [7–14]. Instead, phase diagrams of a simple eutectic type have been suggested by a number of thermodynamic studies and evaluations of the Cu–Cr system. The currently accepted phase diagram is of the eutectic type, which was proposed on the basis of a thermodynamic study with mass spectrometry [14]. Besides an S-shaped liquidus of Cr-rich solid solution, the phase diagram shows a metastable miscibility gap, of which the critical point lies at the Cu-rich side. However, the phase diagram is in conflict with two latest studies. New measurements under

improved conditions [15] showed that the phase diagram has underestimated liquidus temperatures at middle compositions by an amount of 50–150 K. On the other hand, splat-quenching experiments [16] suggested that the critical point of the miscibility gap should lie at the Cr-rich side of the phase diagram. In order to clarify such discrepancies, it is of urgent demand to perform more studies of phase equilibria in the Cu–Cr system.

Electromagnetic levitation processing has proven to be a useful tool for studies of phase equilibria and thermodynamic properties of metallic materials [17, 18], because it eliminates crucible-induced melt contamination. By combining it with pyrometric measurements, Anderson et al. [19] determined liquidus temperatures of Ti–Al alloys with good reproducibility. They also found that the residual oxygen content of the Ti–Al samples is reduced by 100 ppm through electromagnetic levitation processing due to decomposition of the stable oxides into volatile ones and gaseous oxygen at high temperatures. Hence, it is expected that the adoption of electromagnetic levitation processing will bring about the same benefits to studies of phase equilibria in the Cu–Cr system. In this study, the liquidus temperatures over a wide range of Cu–Cr compositions were measured using the same method as that for the Ti–Al system. In terms of the present data, phase equilibria at elevated temperatures were calculated using the CALPHAD method. A novel monotectic type phase diagram was proposed, which reconciles the discrepancies between the literature data.

Materials and methods

Elemental materials of Cu (99.999% purity) and Cr (99.99% purity) were chosen for preparation of master alloys of nominal compositions $Cu_{100-x}Cr_x$ ($x = 10$–70). An excess amount of elemental Cu was added to compensate for mass losses through subsequent melting. The materials were melted using an arc-melting furnace under protection of a Ti-gettered argon atmosphere of 99.999% purity. In order to reach a chemical homogeneity, the ingots were melted few times after they were flipped. The received ingots had masses ranging between 1.537 and 1.710 g. They were processed using electromagnetic levitation for determination of the liquidus temperatures.

In each levitation experiment, an alloy ingot was inserted into the coil of a radio frequency electromagnetic levitation facility, and supported with a hollow sample holder. After evacuation to a vacuum pressure of 6×10^{-4} Pa, the levitation chamber of the facility was backfilled with argon (99.999% purity) to a pressure of 3×10^{4} Pa. The ingot sample was levitated and melted inductively by tuning the power to the coil. The sample was overheated and held for a few minutes to insure complete melting. Then, the sample was cooled by a helium stream of 99.999% purity jetting out of the sample holder. In order to reduce evaporation of elemental Cu, the sample was subjected to one heating–cooling cycle only. The sample temperature was measured using a single-color pyrometer with a relative accuracy of ± 7 K and a response time of 10 ms. The pyrometer was focused onto the sample surface through a horizontal viewport of the levitation facility, because a fume rose from the top surface of the sample. The measured temperature was calibrated with respect to a well-determined eutectic temperature of 1349 K [11, 15]. For each composition, at least four samples were levitated for determination of the liquidus temperatures. For some samples, a thin film of oxides appeared on the surface. The corresponding liquidus temperatures were assumed to have lower reliability.

The solidified samples were weighed using an electric balance with an accuracy of 1 mg. Their mass losses were mainly due to evaporation of elemental Cu during levitation melting. The compositions of the solidified samples were estimated by subtracting the losses from the initial mass of elemental Cu. The samples were mounted in an epoxy resin. After grinding and polishing, their microstructures were examined using scanning electron microscopy (SEM) in the back-scattering mode. Bulk compositions of the samples were measured using energy dispersive X-ray spectrometry (EDS) attached to the SEM, and compared with those estimated from the mass losses. Some of the samples were tested with a TC 436 O/N analyzer for determination of residual oxygen concentrations.

Experimental results

The levitated samples were determined to have a mean mass loss ranging between 0.034 and 0.190 g depending on bulk composition. The higher the nominal Cr concentration x is, the larger the mean mass loss is. Figure 1 shows the estimated and measured Cr concentrations of the samples versus their nominal Cr concentrations, x. There is a reasonable agreement between the two sets of the data. Except for two compositions, the differences between the measured Cr concentrations and the nominal Cr concentrations are within the errors of EDS measurements (typically ± 0.5 at.%). Hence, the control of sample composition with additions of excess Cu to raw materials is effective. For accuracy, the measured compositions are used below.

Figure 2 illustrates cooling curves of the samples. Each curve shows two thermal plateaus. The first one varies greatly with alloy composition, whereas the second one does not change much. Since liquid undercooling is negligible for each sample, the first one, marked by an arrow,

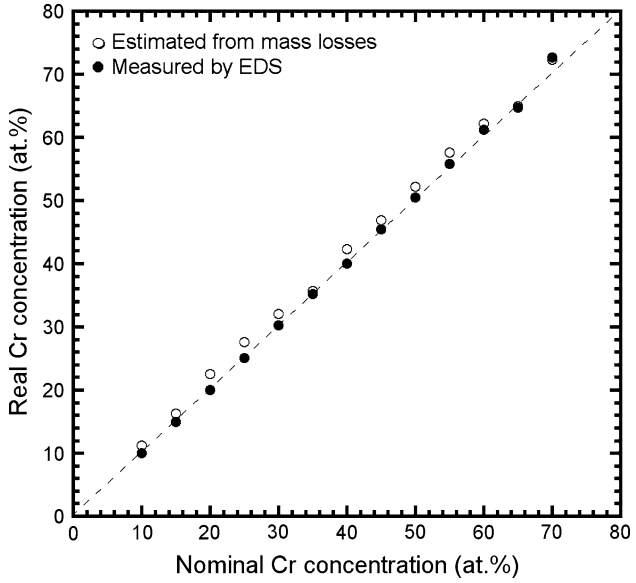

Fig. 1 Estimated and measured Cr concentrations versus nominal Cr concentration of $Cu_{100-x}Cr_x$ samples

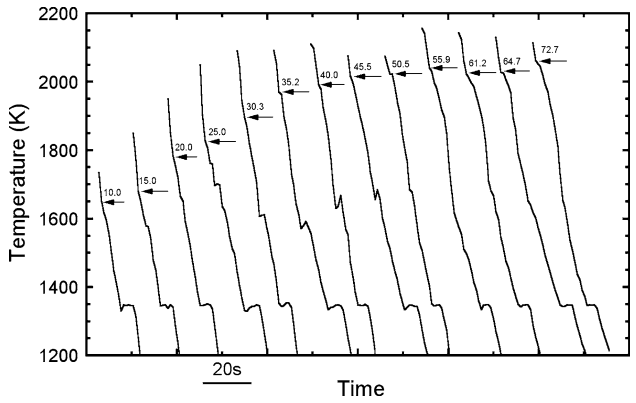

Fig. 2 Illustration of cooling curves of $Cu_{100-x}Cr_x$ samples. *Arrows* show the estimated liquidus temperatures, and figures show the measured x

can be treated as the liquidus temperature approximately. The second one corresponds to the invariant eutectic temperature. Besides the two plateaus, a recalescence-like temperature rise occurs to some samples at an intermediate temperature. This phenomenon can be related to a local change of the emissivity of sample surface caused by formation of a discontinuous oxide layer or by aggregation of Cr-rich dendrites. For samples of low Cr compositions ($x = 10.0$–50.5), the liquidus temperature increases steadily with increasing x. For those of high Cr compositions ($x = 55.9$–72.7), the liquidus temperature tends to level off. In order to reduce experimental errors, the measured liquidus temperatures are averaged over four or more samples for each composition. The averaged liquidus temperatures are listed in Table 1.

Table 1 List of the measured and calculated liquidus temperatures

Cr concentration (at.%)	Measured liquidus temperature (K)	Mean deviation (K)	Calculated liquidus temperature (K)
10.0	1641	±17	1650
15.0	1665	±10	1735
20.0	1773	±9	1803
25.1	1853	±9	1859
30.3	1912	±3	1908
35.2	1950	±10	1946
40.0	1973	±14	1977
45.5	2002	±9	2003
50.5	2010	±20	2019
55.9	2031	±6	2020
61.2	2027	±14	2020
64.7	2022	±10	2020
72.7	2033	±9	2020

Figure 3 illustrates microstructures of the samples. As seen in Fig. 3a, b, compositions ranging between $x = 10.0$ and $x = 50.5$ solidify into a microstructure consisting of Cr-rich dendrites and a Cu-rich matrix. The volume fraction of Cr-rich dendrites increases with increasing x. In contrast, compositions ranging between $x = 55.9$ and $x = 72.7$ solidify into a droplet-shaped microstructure, where Cr-rich dendrites and Cr-rich spheres are embedded in a Cu-rich matrix (see Fig. 3c, d). The Cr-rich spheres are not a single phase, but a mixture of Cr-rich grains and intergranular Cu-rich phase. The volume fraction of Cr-rich spheroids increases with increasing x. The morphology of the Cr-rich spheroids also shows a change. In local regions, the Cr-rich spheres and the surrounding materials are arranged into an interconnected structure (see the inset of Fig. 3d). Due to lack of enough liquid at the end of solidification, holes are seen in the Cu-rich matrix. As explained below, the formation of such a droplet-shaped microstructure provides direct evidence for the existence of a stable miscibility gap in the Cu–Cr system.

As shown in Fig. 4, small faceted Cr_2O_3 particles are segregated between the arms of the Cr-rich dendrites. These particles are likely to act as the substrate for heterogeneous nucleation of primary Cr-rich dendrites, reducing undercoolings of the samples to a negligible level. The oxygen concentrations of the samples were measured. The results are displayed in Fig. 5, showing a linear law with x. A maximum oxygen concentration of 490 ppm was determined at $x = 72.7$. Such a value is well below the oxygen concentration of the electrolytic copper material, typically 600 ppm. It is suggested that electromagnetic levitation processing has lowered oxygen concentrations of the Cu–Cr samples as expected.

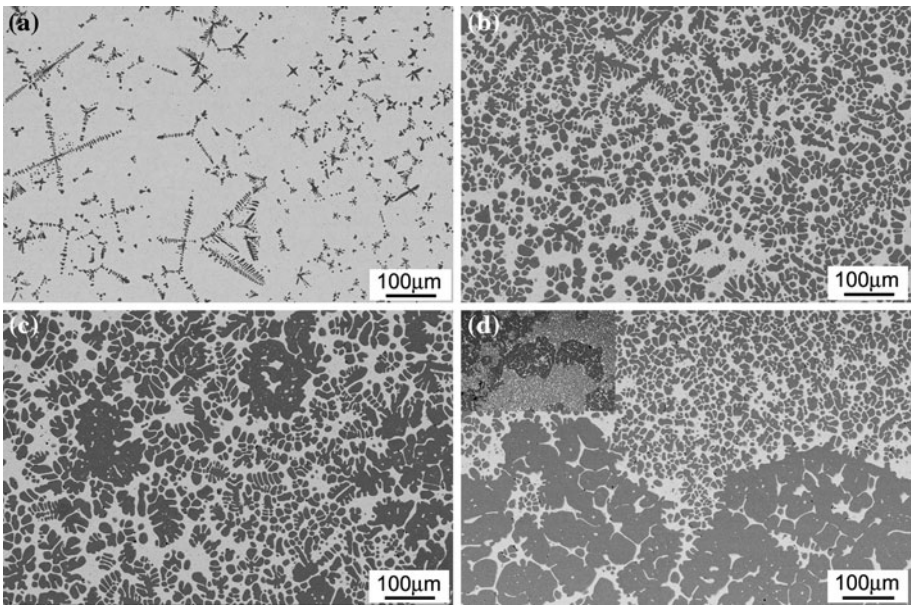

Fig. 3 Back-scattered SEM micrographs illustrating solidification microstructures of $Cu_{100-x}Cr_x$ samples. **a** $x = 10.0$, ***b*** $x = 50.5$, **c** $x = 61.2$, **d** $x = 72.7$. The *inset* in **d** shows an interconnected structure under low magnification

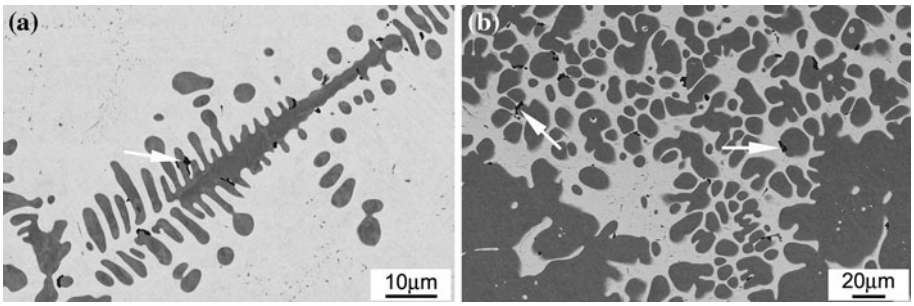

Fig. 4 Back-scattered SEM micrographs illustrating faceted Cr_2O_3 particles segregated between the arms of Cr-rich dendrites in $Cu_{100-x}Cr_x$ samples (see *white arrows*). **a** $x = 10.0$ and **b** $x = 72.7$

Thermodynamic modeling

Phase equilibria in the Cu–Cr system are modeled using the CALPHAD method in terms of the present liquidus temperatures. We assume that the liquid phase can be treated as a subregular solution. Then, the Gibbs free energy of the liquid phase is given by

$$G^{\mathrm{L}} = (1-y)^0G^{\mathrm{L}}_{\mathrm{Cu}} + y^0G^{\mathrm{L}}_{\mathrm{Cr}} + RT[(1-y)\ln(1-y) + y\ln(y)] + (1-y)y\Omega^{\mathrm{L}} \quad (1)$$

where ${}^0G^{\mathrm{L}}_{\mathrm{Cu}}$ and ${}^0G^{\mathrm{L}}_{\mathrm{Cr}}$are the Gibbs free energy of the two elements at the standard reference state [20], y is the mole fraction of elemental Cr, T is temperature, R is the gas constant, Ω^{L} is an interaction parameter of the components in the liquid phase L. We assume that Ω^{L} has the following formalism:

$$\Omega^{\mathrm{L}} = (A - By) - T(C - Dy) \quad (2)$$

where A, B, C, and D are material-dependent constants. When the liquid phase is equilibrated with Cr-rich solid solution, they have equal chemical potentials of both elements, namely:

$$\mu^{\mathrm{L}}_{\mathrm{Cr}} = \mu^{\mathrm{S}}_{\mathrm{Cr}}. \quad (3)$$

The chemical potential of Cr in the liquid phase is obtained by differentiating Eq. 1 with respect to y:

$$\mu^{\mathrm{L}}_{\mathrm{Cr}} = {}^0G^{\mathrm{L}}_{\mathrm{Cr}} + (1-y)^2\Omega^{\mathrm{L}} + RT\ln y + y(1-y)^2\frac{\partial\Omega_{\mathrm{L}}}{\partial y} \quad (4)$$

The solubility of Cu in Cr-rich solid solution is negligible [11]. Thus, the chemical potential of Cr in it is reduced to the Gibbs free energy of pure Cr:

$$\mu^{\mathrm{S}}_{\mathrm{Cr}} = {}^0G^{\mathrm{S}}_{\mathrm{Cr}}. \quad (5)$$

By substituting Eqs. 4 and 5 into Eq. 3, we obtain the following expression

$${}^0G^{\mathrm{S}}_{\mathrm{Cr}} = {}^0G^{\mathrm{L}}_{\mathrm{Cr}} + (1-y)^2\Omega^{\mathrm{L}} + RT\ln y + y(1-y)^2\frac{\partial\Omega_{\mathrm{L}}}{\partial y} \quad (6)$$

The four constants of Eq. 2 can in principle be determined by solving Eqs. 2 and 6 with the measured liquidus temperatures. However, this issue is ill-defined mathematically. In order to overcome it, the measured liquidus temperatures at compositions with $y > 0.20$ are assumed to have higher reliability than that of others. Furthermore, the

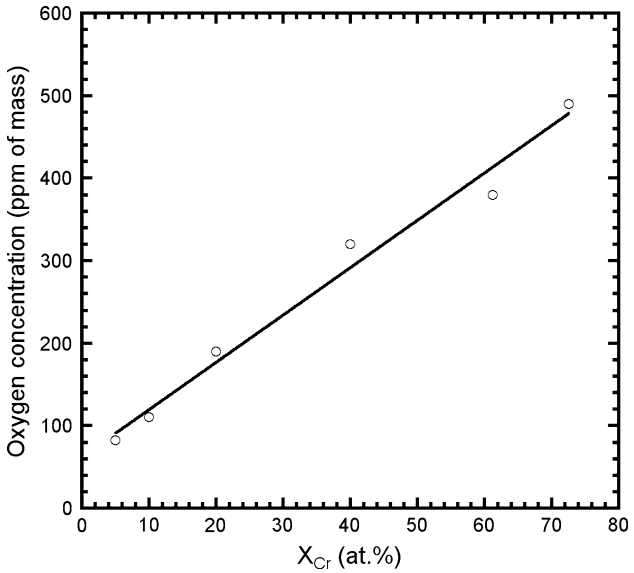

Fig. 5 Measured concentration of oxygen impurity (in ppm weight) versus Cr concentration of $Cu_{100-x}Cr_x$ samples

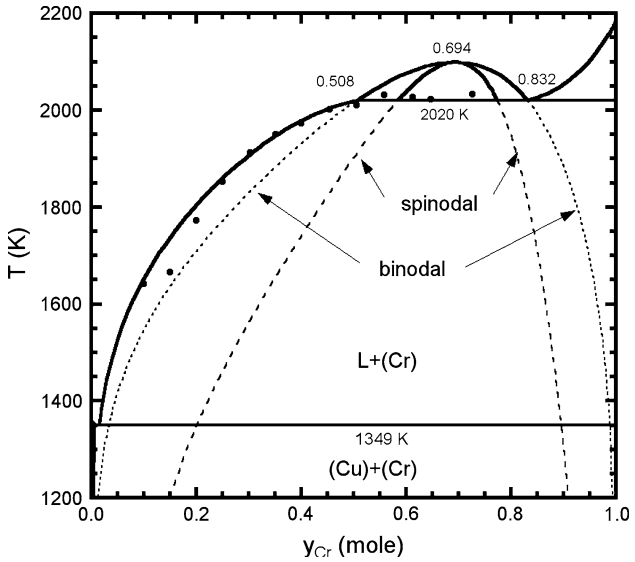

Fig. 6 Illustration of the present monotectic type phase diagram of the Cu–Cr system. The *dashed* and *dotted lines* represent the metastable extensions of the binodal line and of the spinodal line into the undercooled region, respectively

eutectic point and the melting point of 2180 K for pure Cr are chosen as two complementary data, which have been well determined in literature [11, 15]. These data of higher reliability are optimized by fitting to a quintic polynomial. The optimized liquidus temperatures are substituted into Eq. 6 with the data of pure elements by Dinsdale [20]. Applying a least square logarithm, the interaction parameter in the liquid phase, Ω^L, is determined as follows:

$$\Omega^L = (86088 - 10674y) - T(34.39 - 17.05y) \quad (7)$$

By combining Eq. 7 with Eqs. 1 and 3, phase equilibria between the liquid phase and pure Cr are calculated over a wide range of composition and temperature.

The calculated liquidus temperatures are listed in Table 1, and compared with the measured data. A mean deviation of ±22 K is determined. The calculated Gibbs free energy of the liquid phase shows two minima at high temperatures. It is implied that there exists a stable miscibility gap in the liquid state. The boundaries of the miscibility gap are calculated by finding a common tangent line to the Gibbs free energy curve as a function of y numerically. The calculations show that the critical point of the miscibility gap lies at $y = 0.694$ and $T = 2098$ K. The gap spans from $y = 0.508$ to $y = 0.832$, when the liquid is cooled to a monotectic temperature of 2020 K. Based on these results, a novel monotectic type phase diagram is proposed for the Cu–Cr system, as shown in Fig. 6. Because the interaction parameter in the liquid phase is reduced to a similar expression for compositions with $y < 0.0156$, the liquidus temperatures of Cu-rich solid solution are reproduced from a previous assessment of the Cu–Cr system [9].

Discussion

Stability of the liquid miscibility gap

The existence of a stable miscibility gap in the Cu–Cr system has ever been suggested by several research groups [3–6]. However, such a conclusion has been questioned by other researchers in consideration of the use of impure raw materials and contamination of the samples by the crucible materials and reactive atmospheres. In this study, the experimental conditions were improved in all three aspects. In particular, the adoption of electromagnetic levitation processing eliminated crucible-induced melt contamination, and lowered the concentration of residual oxygen impurity of the samples to a level less than 500 ppm. A historic study of the Cu–Nb system [21] demonstrated that a suspected monotectic reaction vanishes when the residual oxygen impurity concentration of as-cast ingots is reduced from 2300 to 760 ppm. Another experimental study [15] suggested that phase equilibria in the Cu–Cr system are not as sensitive to oxygen impurity as are in the Cu–Nb system. Following these studies, we suppose that the level of the residual oxygen impurity of the present samples does not have any critical influence on the stability of the miscibility gap in liquid Cu–Cr alloys.

The effect of cooling rates on the stability of the miscibility gap is also considered. A droplet-shaped microstructure has been generally observed for rapidly solidified Cu–Cr materials [22–25], and interpreted by assuming metastable liquid phase separation in the undercooled liquid. In this study, the cooling rates of the samples ranged

from 50 to 80 K/s, which are by two or more orders smaller than those of the rapidly solidified materials. Meanwhile, the actual undercoolings of the samples are negligible (see Fig. 2). Hence, the droplet-shaped microstructure of the present samples is unlikely to result from metastable liquid phase separation in the undercooled liquid. Rather, it is due to the existence of a stable miscibility gap in the Cu–Cr system.

Reliability of the novel phase diagram

As displayed in Fig. 7, the present phase diagram shows good agreement with different sets of the literature data. First, the liquidus temperatures at low Cr compositions ($y = 0.1$–0.2) agree with many sets of the literature data [6–15, 26, 27]. Second, the liquidus temperatures at compositions between $y = 0.25$ and 0.50 get close to one set of the literature data [6]. Third, the present monotectic temperature agrees well with two sets of the literature data within the experimental errors [5, 6]. Such agreement demonstrates that the present phase diagram has high reliability.

There remain minor discrepancies in the liquidus temperatures at high Cr compositions and in the range of the stable miscibility gap. However, these discrepancies can be understood, if the conditions under which the literature data were produced are considered. The remaining discrepancy in the liquidus temperatures arises mainly from the eutectic type phase diagrams based on thermodynamic studies and assessments of the Cu–Cr system [7–13]. In those studies, the activity data of the liquid phase were measured for temperatures up to 1873 K because of a limited heating capability of the mass spectrometers [14, 26, 27]. According to the present phase diagram, compositions with $y = 0.30$ or above could not be melted completely at 1873 K. The available activity data therefore might not be sufficient enough to give an accurate description of the interaction parameter in the liquid phase at higher temperatures. On the other hand, the liquidus temperatures were often measured at low Cr concentrations. For these reasons, the liquidus temperatures at high Cr compositions are likely to have been underestimated. In a recent study, Li et al. [15] determined liquidus temperatures over a wide range of composition. Because of improved conditions, the measured liquidus temperatures were raised considerably above those predicted by the thermodynamic studies of the system. However, their samples might be contaminated, because a serious reaction between Cu–Cr melts and an Al_2O_3 crucible material had already been observed by other researcher [6]. Hence, it is not surprising that the liquidus temperatures measured by Li et al. [15] are yet lower than those predicted by the present phase diagram.

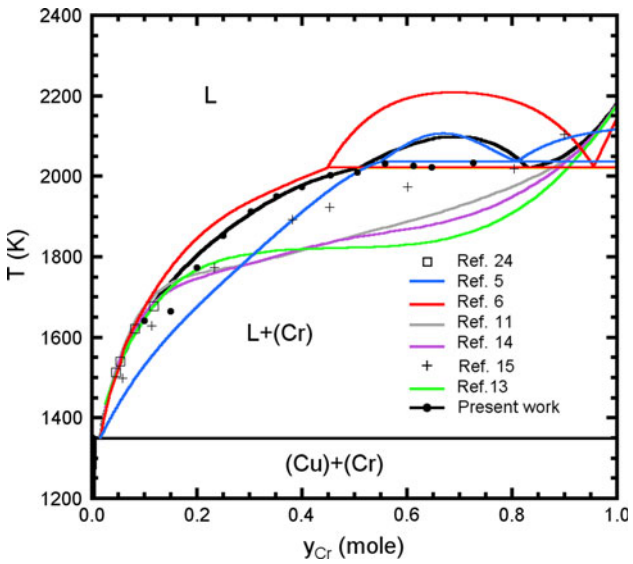

Fig. 7 A comprehensive comparison of the present Cu–Cr phase diagram with the literature data

The discrepancy in the range of the miscibility gap stands with two experimental studies. In one study [6], the samples were melted in a ceramic crucible, and were contaminated by the crucible material. The actual oxygen content of the samples, however, was not determined. In the other study [5], the measured melting point for pure Cr was considerably lower than the well accepted value of 2180 K [28]. Such a difference implies that the used Cr material might have a special impurity, which tends to reduce the melting point of Cr. In a word, the samples in both studies were not pure enough. As a result, the phase equilibria in liquid Cu–Cr alloys might have been shifted, leading either to enlargement or to reduction of the range of the miscibility gap depending on the species and on content of the impurities.

Conclusions

Liquidus temperatures at Cu–Cr compositions ranging from 10.0 to 72.7 at.% Cr have been determined using electromagnetic levitation processing. Microscopic studies have shown that the samples of Cu-rich compositions solidify into a dendritic microstructure, whereas those of Cr-rich compositions solidify into a droplet-shaped microstructure. The observation of the latter type of microstructure has confirmed the existence of a liquid miscibility gap. In terms of the present liquidus temperatures, phase equilibria in the Cu–Cr system have been calculated using the CALPHAD method. The interaction parameter in the liquid phase has been determined as $\Omega^{L} = (86088 - 10674y) - T(34.39 - 17.05y)$. A novel

monotectic type phase diagram has been proposed, which displays a stable miscibility gap over compositions between 50.8 and 83.2 at.% Cr at a monotectic temperature of 2020 ± 22 K. The novel phase diagram has reconciled the discrepancies in the liquidus temperatures and in the range of the miscibility gap between the literature data.

Acknowledgements This study is financially supported by the National Natural Science Foundation of China (50571025 and 50871078) and by the Ministry of Education (NCET05-0292). The authors thank Dr. H. Nagaumi for providing high purity chromium material. The authors also thank Dr. Jingbo Li for discussions. The authors are indebted to Mr. G. Luo for his assistance in experimental work.

References

1. Slade PG (1994) IEEE Trans Compon Packag Manuf Technol 17:96
2. Lee KL (2004) J Mater Sci 39:3047. doi:10.1023/B:JMSC.0000025831.58057.52
3. Hindrichs G (1908) Z Anorg Chem 59:414
4. Siedschlag E (1923) Z Anorg Chem 131:173
5. Leonov M, Bochvar N, Ivanchenko V (1986) Dokl Akad Nauk SSSR 290:888
6. Müller R (1988) Siemens Forsch Entwickl Ber 1:105
7. Kuznetsov GM, Fedorov FN, Rodnyanskayz AL (1977) Sov Non-Ferrous Met Res 3:104
8. Chakrabarti DJ, Laughlin DE (1984) Bull Alloy Phase Diagr 5:59
9. Saunders N (1987) Mater Sci Technol 3:671
10. Hämäläinen M, Jääskeläinen K, Luoma R, Nuotio M, Taskinen P, Teppo O (1990) Calphad 14:125
11. Zeng K, Hämäläinen M (1995) Calphad 19:93
12. Michaelsen C, Gente C, Bormann R (1997) J Mater Res 12:1463
13. Turchanin MA (2006) Powder Metall Metal Ceram 45:457
14. Jacob KT, Priya S, Waseda Y (2000) Z Metallkd 91:594
15. Li D, Robinson MB, Rathz TJ (2000) J Phase Equilib 21:136
16. Zhou ZM, Gao J, Li F, Zhang YK, Wang YP, Kolbe M (2009) J Mater Sci 44:3793. doi:10.1007/s10853-009-3511-y
17. Adachi M, Schick M, Brillo J, Egry I, Watanabe M (2010) J Mater Sci 45:2002. doi:10.1007/s10853-009-4149-5
18. Munitz A, Bamberger M, Venkert A, Landau P, Abbaschian R (2009) J Mater Sci 44:64. doi:10.1007/s10853-008-3115-y
19. Anderson CD, Hofmeister WH, Bayuzick RJ (1993) Metall Trans A 24:61
20. Dinsdale AT (1991) Calphad 15:317
21. Verhoeven JD, Gibson ED (1978) J Mater Sci 13:1576. doi:10.1007/BF00553214
22. Cooper KP, Ayers JD, Malzahn Kampe JC, Feng CR, Locci IE (1991) Mater Sci Eng A 142:221
23. Sun Z, Zhang C, Zhu Y, Zhang C, Yang Z, Ding B, Song X (2003) J Alloys Compd 361:165
24. Zhou ZM, Wang YP, Gao J, Kolbe M (2005) Mater Sci Eng A 398:318
25. Gao J, Wang YP, Zhou ZM, Kolbe M (2007) Mater Sci Eng A 449–451:654
26. One K, Nishi S, Oishi T (1984) Trans Jpn Inst Mater 11:810
27. Timberg L, Toguri JM (1982) J Chem Thermodyn 14:193
28. Andersson JO (1985) Int J Thermodyn 6:411